TEMs BASED COMPOSITES AND ITS PRACTICAL APPLICATIONS

Nikita A. Drozhzhin[1, 2*] (ID), Olga Yu. Ponomareva[1, 2] (ID), Ilya I. Vinogradov[2] (ID),
Genrikh V. Serpionov[2] (ID), Abubakir Kanet[3] (ID), Daria V. Nikolskaya[2] (ID), Tatiana N. Vershinina[1, 2] (ID)

[1]Dubna University, Dubna, Russia;
[2]Joint Institute for Nuclear Research, Dubna, Russia;
[3]Institute of Batteries, Astana, Kazakhstan
(*Corresponding author's e-mail: dna.17@uni-dubna.ru)

Nickel (II) Based Metal-Organic Framework Consolidated on Nanofibers Modified Track-Etched Membrane for Dye Removal

Metal-organic frameworks (MOFs) are promising adsorption agents with many potential applications. However, most experiments exploring the potential applications of MOFs have used powders, which limits the range of possible applications. To solve this problem, an approach to design hybrid membrane (HM) based on track-etched membrane, electrospun nanofibers and MOF based on L-tryptophan, 1,2-bis(4-pyridyl)ethylene and Ni (II) (Ni-MOF) was proposed in the current paper. An investigation of Ni-MOF morphology on hydrophilic chitosan and hydrophobic polyvinylidene fluoride nanofibers showed that the Ni-MOF tends to form superstructures — spherical conglomerates consisting of flaky crystallites on both types of nanofibers. The HMs and Ni-MOF powder were characterized by SEM and PXRD. The adsorption properties of the Ni-MOF powder towards model anionic methyl orange (MO) and cationic rhodamine B (Rh B) including kinetics and isotherm were studied. An investigation of dyes removal by HMs in dead-end filtration mode indicates the effectiveness of MO and Rh B adsorption as high as ~97 % (~380 $\mu g/cm^2$) and ~9 % (~37 $\mu g/cm^2$), respectively. The possibility of regeneration was also investigated. Thus, the HMs may find a potential application for advanced wastewater treatment processes to provide removal of MO in microfiltration mode.

Keywords: track-etched membranes, metal-organic frameworks, hybrid membranes, nanofibers, electrospinning, dye removal, adsorption, water treatment

Introduction

Water pollution caused by industries is one of the most significant global problems. Water may contain numerous hazardous compounds such as dyes, heavy metal ions, or drugs, which pose severe risks to the environment and human health. Methyl Orange (MO), an anionic dye is commonly used in textile, printing industries and in laboratory practice. Despite this, MO is recognized as low biodegradable, toxic, carcinogenic and mutagenic compound. It is reduced into aromatic amines by intestinal microorganisms which can lead to intestinal cancer [1–3]. Rhodamine B (Rh B) is a cationic dye employed in textile, paper, paint industry. It is toxic, carcinogenic and non-biodegradable. The presence of MO or Rh B in water can negatively affect aquatic organisms due to toxicity and ability to inhibit photosynthesis by reducing light penetration [4–7]. Various techniques have been used for removal of dyes from water media: membrane filtration, adsorption, photocatalysis, sedimentation, electrochemical methods and so on. Among them, adsorption is one of the most simple and effective methods for wastewater treatment [8, 9]. Nevertheless, disadvantages of numerous traditional adsorbents are still poor selectivity, retrievability or stability and slow removal rate [10]. Thus, design of novel systems for dye removal is highly demanded.

Metal-organic frameworks (MOFs) are crystalline compounds consisting of metal ions or clusters that are held together by organic ligands. These compounds can form one-, two- or three-dimensional frameworks that may be porous. Since the 1990s and to the present day, they have been attracting great research interest due to the unique properties such as high surface area and tunability of structure [11]. There are a variety of papers studied MOFs as dyes adsorbent. Most experiments of MOFs application in this field were carried out using MOFs powders [12, 13]. However, for improving processability and realization of MOFs practical application in wastewater treatment, depositing MOFs on porous supports to form hybrid membranes (HMs) could be a promising solution [14]. Recent studies have proposed a novel approach to creating functional HMs based on track-etched membranes (TMs) modified by electrospun nanofibers (NFs) layer. This approach has proven suitable for designing materials for removal of harmful ions and dyes from wastewater, seawater desalination processes and wound dressings [9, 15–19].

Herein we present an approach to design novel hybrid membrane based on nanofiber-modified track-etched membrane and MOF synthesized via a low temperature solvothermal method. The MOF based on L-tryptophan, 1,2-bis(4-pyridyl)ethylene and Ni (II) (Ni-MOF) as it can be synthesized under mild conditions that exclude membrane damage. TMs modified with chitosan (Ch) and polyvinylidene fluoride (PVDF) NFs were used as models of hydrophilic and hydrophobic substrates, respectively. The well-defined pore architecture and thoroughly studied physicochemical properties make it possible to use TMs as a convenient model for investigating the processes of designing HMs. To study the adsorption performance two dyes, anionic methyl orange and cationic rhodamine B, were selected as model compounds. The adsorption characteristics such as kinetics and isotherms of adsorption by the Ni-MOF powder were investigated. Dye removal by HMs in filtration mode and regeneration potential were evaluated. Schematically the synthesis process and application in dye adsorption of HMs is illustrated in Figure 1.
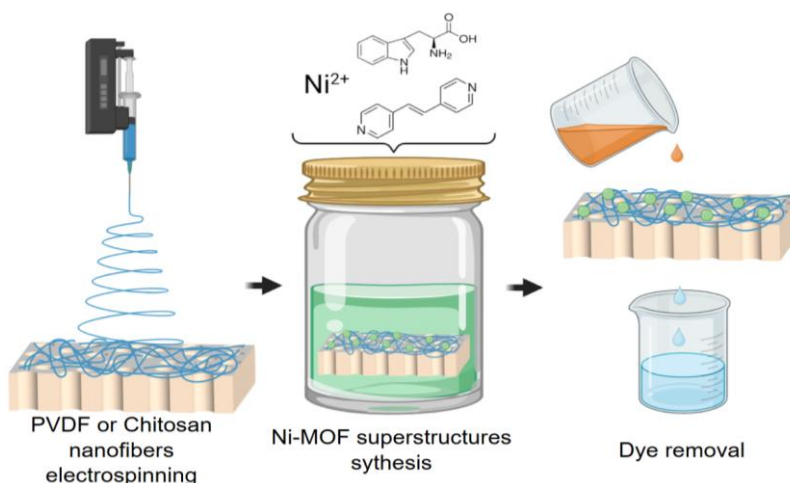

Figure 1. Schematic illustration of HMs preparation and application process

Experimental

Materials

Polyethylene terephthalate (PET) TM with a thickness of 23 μm, pores diameter of 0.3 μm and pores density of $(2.7\pm0.3)\times10^8$ cm^{-2} was made from Hostaphan RNK film in Flerov Laboratory of Nuclear reactions of Joint Institute for Nuclear Research. This membrane was covered by 40 ± 4 nm thick Ti layer in Ivtekhnomash, LLC and used as a support for future studies [20]. The titanium layer is used as collecting electrode during the electrospinning process to improve uniformity and adhesion of NFs to the TM surface [16, 17].

The following reagents were used: chitosan ($M_w = 200000$ g/mol), polyethylene oxide ($M_w = 300000$ g/mol), 99.8 % acetic acid, 25 % glutaraldehyde, polyvinylidene fluoride ($M_w = 600000$ g/mol), 99.8 % dimethylformamide, 99.8 % acetone were used for electrospinning of NFs; L-tryptophan (98 %), 1,2-bis(4-pyridyl)ethylene (97 %), nickel nitrate (Ni(NO$_3$)$_2$·6H$_2$O, chemically pure), methanol (analytical grade) were used for Ni-MOF synthesis; methyl orange (97 %), rhodamine B (95 %), deionized Milli-Q water, acetate buffer were used for adsorption investigations.

Nanofibers Electrospinning

Ch and PVDF NFs were electrospun on the TM surface according to the methods reported previously [16, 19]. Membranes with Ch or PVDF NF layers were designated as TM+Ch and TM+PVDF, respectively. Density of NFs layer was found to be 0.37±0.03 mg/cm^2 for TM+Ch and 0.55±0.05 mg/cm^2 for TM+PVDF.

Ni-MOF Synthesis

The method described previously was used for synthesis Ni-MOF as a powder and on the membrane surface [21, 22]. Membranes modified by Ni-MOF were marked as TM+Ch+Ni-MOF or TM+PVDF+Ni-MOF. The density of Ni-MOF on the membrane surface was amounted to be 3.4±0.6 mg/cm^2 for TM+Ch+Ni-MOF and 3.8±0.5 mg/cm^2 for TM+PVDF+Ni-MOF.

Characterization Techniques

The morphology of the membranes was studied by scanning electron microscopy (SEM, Hitachi S-3400N). The crystal structure was analyzed by powder X-ray diffraction (PXRD) using PANalytical Empyrean powder diffractometer (CoKα radiation) with a high-efficiency Pixel3D position-sensitive detector at a tube voltage of 40 kV and a current of 40 mA. The 2θ angle range was from 8° to 50° with steps Δθ = 0.026°. Hydrophobic-hydrophilic properties of membranes were estimated by water contact angle measurements using DSA-100. The Brunauer–Emmett–Teller specific surface area of the Ni-MOF powder was measured as 4.5 m^2/g (N$_2$, ASAP 2020).

Adsorption Experiments

Two dyes were selected for adsorption experiments: anionic methyl orange and cationic rhodamine B. For batch adsorption experiments the Ni-MOF powder was used. Adsorption kinetics was studied in duplicate by 15 mg of Ni-MOF in 10 ml of dye aqueous solution with initial concentration 50 mg/L for MO and 10 mg/L for Rh B at 23 °C. Dyes solutions were analyzed by UV-Vis spectrophotometer (Evolution 600) and the adsorption capacity at certain time (q_t, mg/g) was calculated using Eq (1):

$$q_t = \frac{(C_0 - C_t)V}{m}, \tag{1}$$

where C_0 is the initial concentration (mg/L), C_t is the concentration after adsorption for a certain time (mg/L), V is a solution volume (L), m is an adsorbent mass (g). To quantify the adsorption kinetics pseudo-first-order (PFO) model (Eq 2) and pseudo-second-order (PSO) model (Eq 3) were used to fit the experimental data:

$$q_t = q_e \left(1 - e^{-k_1 t}\right); \tag{2}$$

$$q_t = \frac{q_e^2 k_2 t}{1 + q_t k_2 t}, \tag{3}$$

where q_e is the adsorption capacity at equilibrium (mg/g), k_1 is the rate constant of the PFO model (1/min), k_2 is the rate constant of the PSO model (g/mg·min), t is the time (min).

The adsorption isotherm measurements were performed in duplicate by varying the initial dye concentration from 10 to 300 mg/L for MO and from 1 to 30 mg/L for Rh B. Three the most widely applied isotherm models, Langmuir (Eq 4), Freundlich (Eq 5) and Temkin (Eq 6) were employed to fit the experimental data:

$$q_e = \frac{q_{max} K_L C_e}{1 + K_L C_e}; \tag{4}$$

$$q_e = K_F C_e^{1/n}; \tag{5}$$

$$q_e = q_{max} \frac{RT}{b} ln\,(K_T\,C_e), \tag{6}$$

where q_{max} is a monolayer capacity of Ni-MOF (mg/g), K_L is the Langmuir adsorption constant (L/mg), C_e is the concentration at equilibrium (mg/L), K_F is the Freundlich adsorption constant ((mg/g)·(L/ mg)$^{1/n}$), n is an exponent of the Freundlich model, b is the Temkin isotherm constant (J/mol), K_T is the Temkin adsorption constant (L/mg).

The fitting quality and error analysis of the models were carried out by calculating chi-squared parameter (Eq 7) and hybrid fractional error function (Eq 8):

$$\chi^2 = \sum_{i=1}^{n} \frac{\left(q_{cal} - q_{exp}\right)^2}{q_{exp}} \; ; \tag{7}$$

$$HYBRID = \frac{100}{n-p} \sum_{i=1}^{n} \frac{(q_{exp} - q_{cal})^2}{q_{exp}} \; , \tag{8}$$

where q_{cal} is the calculated adsorption capacity (mg/g), q_{exp} is the experimental adsorption capacity (mg/g), n is a number of measured experimental points, p is a number of variable parameters in the equation.

For adsorption investigations in dead-end filtration mode the 25 mm membrane (working diameter 22 mm) was installed in a polycarbonate filter holder. Using tubes, the holder was connected to the syringe containing 30 ml of selected dye with initial concentration 50 mg/L. The syringe was placed into a syringe pump and flow rate was set as 2 ml/min. The solution passed through the membrane was collected in a beaker and placed back into the syringe. The described procedure was repeated throughout 2, 4, 8 and 12 cycles. The adsorption losses as a, % and A, µg/cm^2 was calculated using Eq (9, 10):

$$a = \frac{C_0 - C_n}{C_0} \times 100 \; ; \tag{9}$$

$$A = \frac{(C_0 - C_n)V}{S} \; , \tag{10}$$

where C_n is the concentration after a certain cycle (mg/L), S is a membrane working area (cm^2).

For regeneration studies, the membrane was kept in the 10 ml MO solution with concentration of 50 mg/L for 24 hours. After that the membrane was immersed in acetate buffer solution with pH = 4 for 3 hours. Adsorption (E_A, %) and desorption efficiencies (E_D, %) were calculated throughout 3 adsorption-desorption cycles using Eq (11, 12):

$$E_A = \frac{m_{ads}}{m_0} \times 100 \; ; \tag{11}$$

$$E_D = \frac{m_{des}}{m_{ads}} \times 100 \; , \tag{12}$$

where m_{ads} is the mass of adsorbed MO (µg), m_0 is the initial mass of MO (µg), m_{des} is the mass of desorbed MO (µg).

Results and Discussion

Characterization

The surface morphology of TMs modified by Ch and PVDF was described in detail previously [16, 17, 19]. Both Ch and PVDF NFs on the TM surface possess a smooth and uniform morphology. The average diameters of the NFs calculated by the Gaussian approximation were 164±4 nm for Ch NFs and 216±18 nm for PVDF NFs (Fig. 2 *a*, *b*). After Ni-MOF synthesis on the membranes, superstructures — spherical conglomerates consisting of flaky crystallites, were formed (Fig. 2 *c*, *d*). Average diameter of Ni-MOF superstructures was measured as 19±2 µm for the TM+Ch+Ni-MOF and 22±2 µm for the TM+PVDF+Ni-MOF samples. The results suggest that the morphology of superstructures is independent of the hydrophobic-hydrophilic properties of the substrate.

To confirm that the crystal structure of Ni-MOF is identical in powder form and on the membrane surface, PXRD analysis was performed. As shown in Figure 3, the patterns of the TM+Ch, TM+PVDF, TM+Ch+Ni-MOF and TM+PVDF+Ni-MOF samples contain an amorphous halo in the region up to 20° and the twin peak around 27° and 30° was interpreted as PET [18]. The remaining peaks for the TM+Ch+Ni-MOF and TM+PVDF+Ni-MOF membranes correspond to Ni-MOF [21, 22]. No significant differences were observed between patterns of the Ni-MOF powder and the HMs. Thus, successful deposition of Ni-MOF on the TMs modified by Ch and PVDF NFs was achieved.
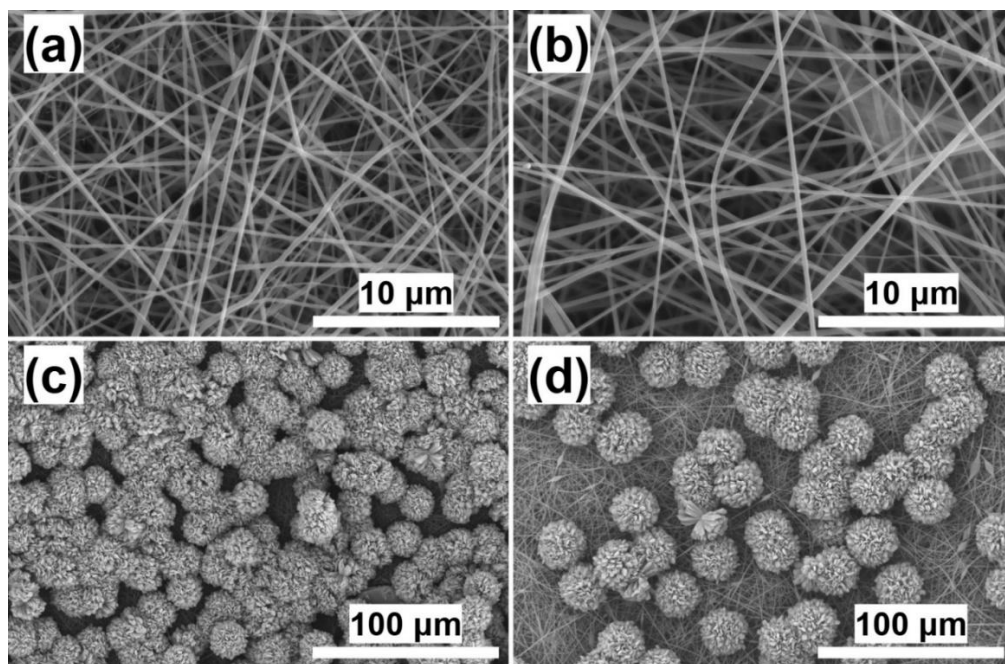
Figure 2. SEM images: (*a*) TM+Ch membrane, (*b*) TM+PVDF membrane,
(*c*) hybrid TM+Ch+Ni-MOF membrane, (*d*) hybrid TM+PVDF+Ni-MOF membrane
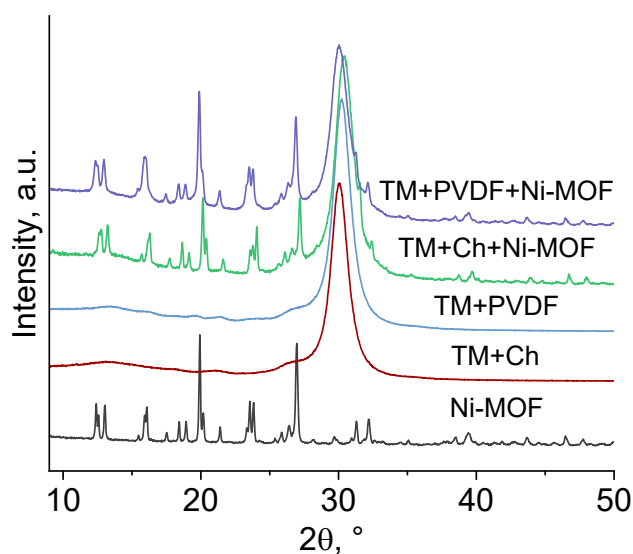

Figure 3. PXRD patterns of Ni-MOF powder, TM+Ch and TM+PVDF membranes,
hybrid TM+Ch+Ni-MOF and TM+PVDF+Ni-MOF membranes

To determine hydrophobic-hydrophilic properties of the HMs and substrates, the water contact angle (CA) measurements were performed (Fig. 4). It was found that the synthesizing Ni-MOF on the membrane's surface increases its hydrophilic properties. The CA of TM+Ch was difficult to measure due to the rapid adsorption of water droplets caused by the NFs. However, this value was estimated as ~15° (Fig. 4, *a*). The synthesis of Ni-MOF on the surface leads to complete wettability of the HM surface (Fig. 4, *b*). The CA of TM+PVDF was measured as 140±1° that determines the membrane surface as hydrophobic (Fig. 4, *c*). The modified sample TM+PVDF+Ni-MOF showed the CA value of 123±9° (Fig. 4, *d*). The relatively large deviation suggests non-uniform coverage of Ni-MOF on the TM+PVDF surface. However, the CA of TM+PVDF+Ni-MOF was decreased up to 20 % in comparison with the pristine one.
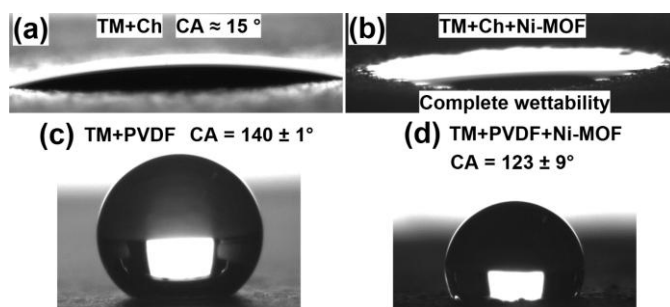
Figure 4. Photos of a water droplet on membranes: (*a*) TM+Ch membrane, (*b*) hybrid TM+Ch+Ni-MOF membrane, (*c*) TM+PVDF membrane, (*d*) hybrid TM+PVDF+Ni-MOF membrane

Dye Adsorption

To explore the adsorption characteristics of the Ni-MOF powder and hybrid membranes HMs, two model contaminants were selected: anionic MO and cationic Rh B. Firstly, adsorption kinetics of the Ni-MOF powder was studied. As shown in Figure 5 the curve reaches a plateau through 120 minutes, corresponding to 95.1±0.1 % MO removal. The time taken for Rh B to reach equilibrium was also estimated as 120 minutes, corresponding to 8.4±1.2 % Rh B removal. The adsorption kinetics was evaluated using the PFO and PSO models. For both MO and Rh B, the adsorption process kinetics were well fitted by the PSO model characterized by the lowest χ^2 values and relatively small deviations between the experimental and calculated adsorption capacities (Table 1). Therefore, the adsorption of MO and Rh B was proportional to the square of the dye concentration and probably based on chemical interactions [23, 24].
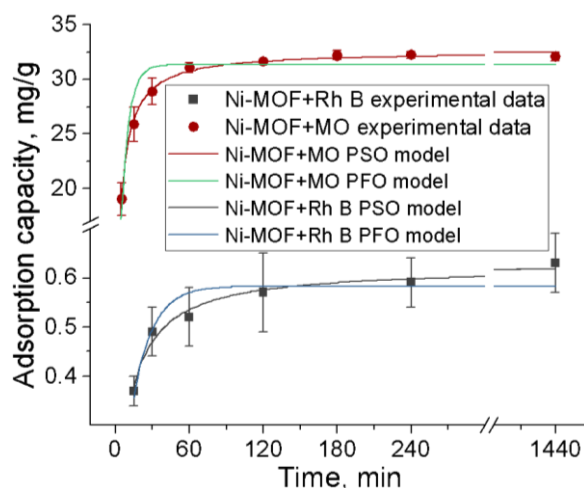

Figure 5. Adsorption kinetics curves of MO and Rh B by Ni-MOF powder

T a b l e 1

Adsorption kinetics model parameters of Ni-MOF powder

Dye	Pseudo-first-order model					Pseudo-second-order model				
	$q_{e, exp}$	$q_{e, cal}$	k_1	χ^2	*HYBRID*	$q_{e, exp}$	$q_{e, cal}$	k_2	χ^2	*HYBRID*
MO	32.1	31.3	0.16	0.6896	9.8514	32.1	32.6	0.0085	0.0188	0.2685
Rh B	0.6	0.58	0.063	0.0092	0.2296	0.6	0.62	0.16	0.0018	0.0453

Adsorption isotherms were evaluated for future investigations. As shown in Figure 6, the adsorption capacity increases with the dye concentration increasing that typical property of many adsorbents. The maximum experimental adsorption capacity toward MO was amounted to be 120.2±1.5 mg/g at initial MO concentration of 300 mg/L. However, the adsorption capacity did not reach its plateau within the studied concentration range. Thus, there are still adsorption sites which can be occupied by MO. The maximum experi-

mental adsorption capacity of Rh B removal was significantly lower and amounted to be 0.67 ± 0.11 mg/g. The adsorption curve reached saturation at dye concentration of 10 mg/L.

For better understanding of the adsorption process, isotherms were fitted by Freundlich, Langmuir and Temkin models. It should be noted that employment of Temkin isotherm requires the q_{max} value. Herein q_{max} value was derived from the Langmuir model [27]. The order of the χ^2 and *HYBRID* values of the models corresponded to the following trend: Freundlich > Langmuir > Temkin for MO and Freundlich > Temkin > Langmuir for Rh B contaminant (Table 2). Freundlich isotherm suggests heterogeneity of adsorbent surface and exponential distribution of binding sites energies [25]. Seen in Table 2, the Freundlich model exhibited the highest χ^2 and *HYBRID* values for both contaminants which indicates that the model is not capable of adequately describing the experimental data. The values of χ^2 and *HYBRID* calculated for the Langmuir model are lower in the comparison with the Freundlich model. Therefore, the assumption of uniformly distributed binding energies and constant adsorption heat is more favorable for the experimental data [26]. The calculated Langmuir maximum adsorption capacity for MO was 115.9 mg/g that is less than the experimental value by ~4 %. This may be caused by an implicit plateau. The best fit of the MO adsorption experimental data was obtained for the Temkin model. The Temkin isotherm assumes uniform distribution of binding energies and linearly decreasing of the adsorption heat along with surface coverage. A value of $b > 0$ constant associated with the heat of adsorption indicates that the process is exothermic [27]. The best fit of the Rh B adsorption experimental data was obtained for the Langmuir model. The calculated Langmuir maximum adsorption capacity for Rh B was 0.74 mg/g that is higher than the experimental value by ~10 %.
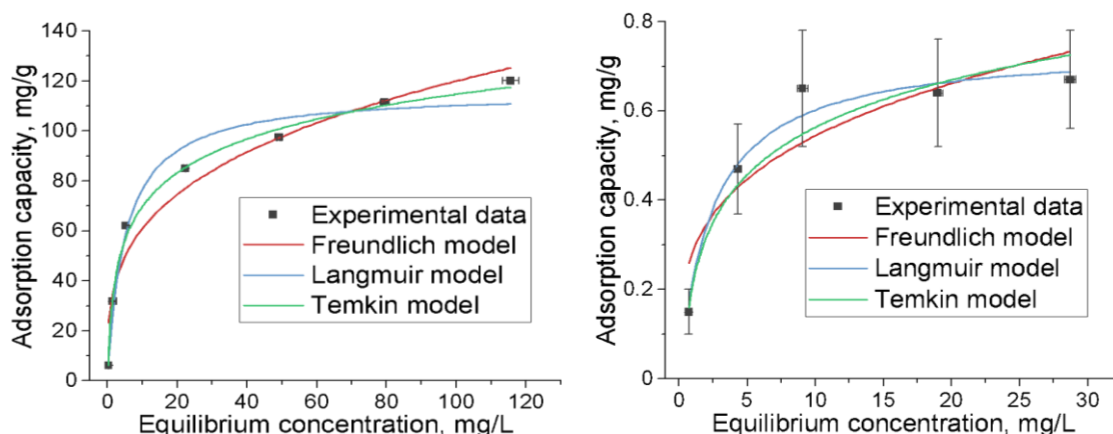

Figure 6. Adsorption isotherms of MO and Rh B by Ni-MOF powder

T a b l e 2

Adsorption isotherm model parameters of Ni-MOF powder

Dye	Freundlich model				Langmuir model				
	K_F	n	χ^2	*HYBRID*	$q_{m, exp}$	$q_{m, cal}$	K_L	χ^2	*HYBRID*
MO	30.7	3.4	51.4495	1028.9902	120.2	115.9	0.19	3.6965	73.9302
Rh B	0.28	3.5	0.1112	3.7056	0.67	0.74	0.42	0.0106	0.3521

Dye	Temkin model			
	b	K_T	χ^2	*HYBRID*
MO	14560	3.5	0.6533	13.0669
Rh B	11865	3.9	0.0246	0.8190

In summary, the Ni-MOF powder is characterized by relatively slow kinetics of dye adsorption (~2 hours). The PSO model was found to be able to adequately describe the experimental data. This may suggest that the adsorption process is chemical in nature. The Temkin model could adequately describe the Ni-MOF dye adsorption isotherms. Thus, the adsorption occurs on uniformly distributed binding sites. At an initial dye concentration of 10 mg/L, the experimental adsorption capacities were approximately ~6 mg/g for anionic MO and ~0.6 mg/g for cationic Rh B. These results suggest that Ni-MOF might exhibits selectivity towards MO.
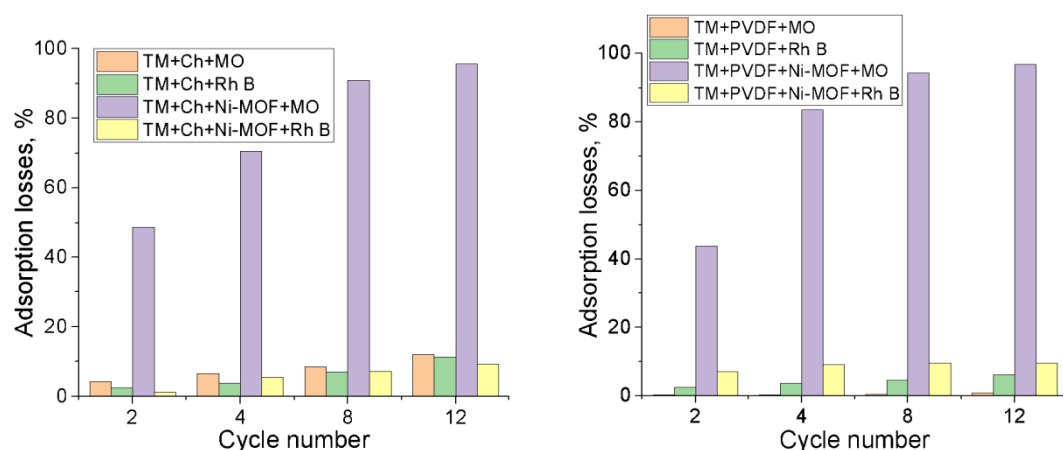
Figure 7. Adsorption loses of MO and Rh B at passing through membranes

The efficiency of dye removal by HMs was studied in dead-end filtration mode. The results are shown in Figure 7. The highest values of adsorption losses were observed for the TM+Ch+Ni-MOF and TM+PVDF+Ni-MOF samples. After 12 cycles, the adsorption losses of MO were 95.7 % for TM+Ch+Ni-MOF and 96.8 % for TM+PVDF+Ni-MOF which corresponds to the specific adsorption losses value of 380.3 μg/cm^2 and 382.2 μg/cm^2, respectively. The differences in the adsorption kinetics of TM+Ch+Ni-MOF and TM+PVDF+Ni-MOF may be caused by the higher density of the Ni-MOF layer on the TM+PVDF+Ni-MOF surface. The adsorption losses of Rh B were significantly less: 9.3 % (36.7 μg/cm^2) for TM+Ch+Ni-MOF and 9.4 % (37.1 μg/cm^2) for TM+PVDF+Ni-MOF. Thus, the adsorption follows the above-mentioned trend: the adsorption of MO is more active than that of Rh B. To estimate the influence of the porous support on the adsorption, the dye removal by TM+Ch and TM+PVDF was studied. The adsorption losses of MO and Rh B on TM+Ch were 12.1 % (47.6 μg/cm^2) and 11.4 % (45.1 μg/cm^2), respectively. The TM+PVDF membrane showed lower maximum adsorption losses values of 0.9 % (3 μg/cm^2) and 6.1 % (24.2 μg/cm^2) for MO and Rh B. Therefore, the Ni-MOF layer mainly contributes to the adsorption of MO by the HMs.
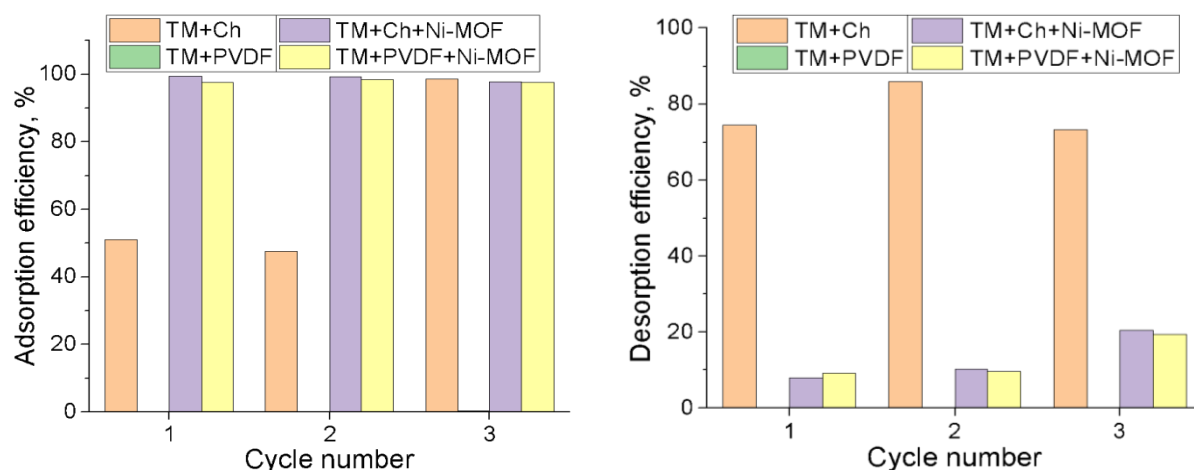

Figure 8. The efficiency of adsorption and desorption of MO by membranes

Batch adsorption-desorption experiments were used to investigate the possibility of regeneration for MO only. The results are shown in Figure 8. The adsorption efficiency of HMs was consistently high during the experiments and amounted to an average of 98.8±0.9 % (127.1±2.2 μg/cm^2) for TM+Ch+Ni-MOF and 97.9±0.5 % (125.9±1 μg/cm^2) for TM+PVDF+Ni-MOF. The desorption efficiency of HMs was ~10 % during 2 cycles and doubled by the 3rd cycle. The desorption efficiency increase may mean degradation of the Ni-MOF crystal structure during adsorption-desorption cycles. The adsorption efficiency of the TM+Ch membrane was 49.3±2.5 % (63.3±3.8 μg/cm^2) during 2 cycles and reached 98.5 % (125.7 μg/cm^2) by the 3rd cycle. This result may indicate the process of chitosan swelling which leads to the reduction in the degree of crosslinking and increasing in the number of binding sites. The average desorption efficiency of the TM+Ch

membrane was 77.9 ± 7 % during the experiments. No adsorption and desorption activity of the TM+PVDF membrane was observed. Summing up, the highest values of adsorption efficiency were measured for HMs while the desorption efficiency was relatively low. Nevertheless, the HMs are able to provide effective dye removal within 3 cycles.

Conclusions

In summary, the design of HMs based on Ch and PVDF NFs modified TMs and Ni-MOF was successfully implemented. Morphology, structure and performance parameters of HMs were investigated. It was found that Ni-MOF has an ability to form uniform superstructures with average diameter ~20 μm on the surface of hydrophilic Ch and hydrophobic PVDF NFs. The adsorption characteristics were studied both for the Ni-MOF powder and for HMs. The adsorption process was best described by the PSO kinetic model for both contaminants, while the Temkin isotherm fitted well for MO, and the Langmuir isotherm was more suitable for Rh B. The Ni-MOF powder exhibited maximum experimentally found adsorption capacity towards MO and Rh B as high as 120.2 ± 1.5 mg/g (at 300 mg/L of initial concentration) and 0.67 ± 0.11 mg/g (at 30 mg/L of initial concentration), respectively. The adsorption measurements in dead-end filtration mode showed maximum values of dye adsorption by HMs as high as ~97 % (~380 μg/cm^2) for MO and ~9 % (~37 μg/cm^2) for Rh B. Investigations of regeneration possibilities have shown that the HMs are able to provide effective dye removal within 3 cycles. This study demonstrates an approach to design practical HMs for the application in wastewater treatment. It can be noted that the described approach might be used in the future to design innovative and processable materials for wound healing, racemic mixtures separation and sensing applications.

Funding

Author Information*

―――――――――――――――――――――――――――――――――――――

The authors' names are presented in the following order: First Name, Middle Name and Last Name

Nikita Alekseevich Drozhzhin (*corresponding author*) — PhD Student, Department of Chemistry, New Technologies and Materials, Dubna University, Universitetskaya Street, 19, 141982, Dubna, Russia; Engineer, Joint Institute for Nuclear Research, Joliot-Curie Street, 6, 141980, Dubna, Russia; e-mail: dna.17@uni-dubna.ru; https://orcid.org/0009-0008-5687-5822

Olga Yuryevna Ponomareva — Candidate of Chemical Sciences, Researcher, Joint Institute for Nuclear Research, Joliot-Curie Street, 6, 141980, Dubna, Russia; e-mail: oyuivanshina@mail.ru; https://orcid.org/0000-0001-8551-5246

Ilya Igorevich Vinogradov — Candidate of Chemical Sciences, Head of sector, Joint Institute for Nuclear Research, Joliot-Curie Street, 6, 141980, Dubna, Russia; e-mail: ily7345@gmail.com; https://orcid.org/0000-0002-3056-2165

Genrikh Vladimirovich Serpionov — Candidate of Biological Sciences, Researcher, Joint Institute for Nuclear Research, Joliot-Curie Street, 6, 141980, Dubna, Russia; e-mail: genrihserpionov@gmail.com; https://orcid.org/0009-0001-4545-8811

Abubakir Kanet — Researcher, Institute of Batteries, Kabanbay Batyr Avenue, 53, Z00X8P9, Astana, Kazakhstan; e-mail: kanet707vhs@gmail.com; https://orcid.org/0009-0006-7914-6628

Daria Vladimirovna Nikolskaya — Engineer, Joint Institute for Nuclear Research, Joliot-Curie Street, 6, 141980, Dubna, Russia; e-mail: nikolskaya@jinr.ru; https://orcid.org/0009-0004-2181-1002

Tatiana Nikolaevna Vershinina — Candidate of Physical and Mathematical Sciences, Senior Researcher, Joint Institute for Nuclear Research, Joliot-Curie Street, 6, 141980, Dubna, Russia; e-mail: vershinina@nf.jinr.ru; https://orcid.org/0000-0002-7748-5443

Author Contributions

The manuscript was written through contributions of all authors. All authors have given approval to the final version of the manuscript. CRediT: **Nikita Alekseevich Drozhzhin** investigation, methodology, visualization, writing-original draft; **Olga Yuryevna Ponomareva** conceptualization, investigation, methodology, validation, editing; **Ilya Igorevich Vinogradov** conceptualization, investigation, methodology, validation, editing; **Genrikh Vladimirovich Serpionov** investigation, methodology, validation; **Abubakir Kanet** investigation, methodology, editing; **Daria Vladimirovna Nikolskaya** investigation, methodology; **Tatiana Nikolaevna Vershinina** investigation, editing.

Acknowledgments

Conflicts of Interest

The authors declare no conflict of interest.

Notes

The graphical abstract was created in BioRender.

References

1   Farhan Hanafi, M., & Sapawe, N. (2020). A review on the water problem associate with organic pollutants derived from phenol, methyl orange, and remazol brilliant blue dyes. *Materials Today: Proceedings*, 31, A141–A150. https://doi.org/10.1016/J.MATPR.2021.01.258

2   Habtemariam, T. H., Raju, V. J. T., & Chebude, Y. (2023). Pillared-Layer Metal-Organic Frameworks (MOFs) for Photo-degrada-tion of Methyl Orange in Wastewater. *Advanced Optical Materials, 11*(10). https://doi.org/10.1002/adom.202202843

3   Kishor, R., Purchase, D., Saratale, G. D., Romanholo Ferreira, L. F., Hussain, C. M., Mulla, S. I., & Bharagava, R. N. (2021). Degradation mechanism and toxicity reduction of methyl orange dye by a newly isolated bacterium Pseudomonas aeruginosa MZ520730. *Journal of Water Process Engineering, 43*, 102300. https://doi.org/10.1016/J.JWPE.2021.102300

4   Ali, I., Burakova, I., Galunin, E., Burakov, A., Mkrtchyan, E., Melezhik, A., Kurnosov, D., Tkachev, A., & Grachev, V. (2019). High-Speed and High-Capacity Removal of Methyl Orange and Malachite Green in Water Using Newly Developed Mesoporous Carbon: Kinetic and Isotherm Studies. *ACS Omega, 4*(21), 19293–19306. https://doi.org/10.1021/acsomega.9b02669

5   Behera, A. K., Shadangi, K. P., & Sarangi, P. K. (2024). Efficient removal of Rhodamine B dye using biochar as an adsorbent: Study the performance, kinetics, thermodynamics, adsorption isotherms and its reusability. *Chemosphere, 354*, 141702. https://doi.org/10.1016/J.CHEMOSPHERE.2024.141702

6   Ghibate, R., Senhaji, O., & Taouil, R. (2021). Kinetic and thermodynamic approaches on Rhodamine B adsorption onto pome-granate peel. *Case Studies in Chemical and Environmental Engineering, 3*, 100078. https://doi.org/10.1016/J.CSCEE.2020.100078

7   Oladoye, P. O., Kadhom, M., Khan, I., Hama Aziz, K. H., & Alli, Y. A. (2024). Advancements in adsorption and photodegradation technologies for Rhodamine B dye wastewater treatment: fundamentals, applications, and future directions. *Green Chemical Engineering, 5*(4), 440–460. https://doi.org/10.1016/J.GCE.2023.12.004

8   Bal, G., & Thakur, A. (2022). Distinct approaches of removal of dyes from wastewater: A review. *Materials Today: Proceed-ings*, 50, 1575–1579. https://doi.org/10.1016/J.MATPR.2021.09.119

9   Bode-Aluko, C. A., Pereao, O., Ameh, A. E., Omoniyi, E., Nechaev, A., & Petrik, L. (2025). Removal of rhodamine 6G from aqueous solution in a continuous mode using nano-micro composite membranes. *Nano Trends, 9*, 100096. https://doi.org/10.1016/J.NWNANO.2025.100096

10 Xiang, W., Wang, Q., Li, Z., Dong, J., Liu, J., Zhang, L., Xia, T., He, Y., & Zhao, D. (2024). Water-stable methyl-modified MOF and mixed matrix membrane for efficient adsorption and separation of cationic dyes. *Separation and Purification Technology, 330*, 125268. https://doi.org/10.1016/J.SEPPUR.2023.125268

11 Jiao, L., Seow, J. Y. R., Skinner, W. S., Wang, Z. U., & Jiang, H. L. (2019). Metal–organic frameworks: Structures and functional applications. *Materials Today, 27*, 43–68. https://doi.org/10.1016/J.MATTOD.2018.10.038

12 Ramírez, D. J., Alfonso Herrera, L. A., Colorado-Peralta, R., Rodríguez, R. P., Camarillo Reyes, P. K., Chiñas, L. E., Sánchez, M., & Rivera, J. M. (2021). Highly efficient methyl orange adsorption by UV-012, a new crystalline Co(II) MOF. *CrystEngComm, 23*(19), 3537–3548. https://doi.org/10.1039/D0CE00741B

13 Sağlam, S., Türk, F. N., & Arslanoğlu, H. (2023). Use and applications of metal-organic frameworks (MOF) in dye adsorption: Review. *Journal of Environmental Chemical Engineering, 11*(5), 110568. https://doi.org/10.1016/J.JECE.2023.110568

14 Huang, J., Huang, D., Zeng, F., Ma, L., & Wang, Z. (2021). Photocatalytic MOF fibrous membranes for cyclic adsorption and degradation of dyes. *Journal of Materials Science, 56*(4), 3127–3139. https://doi.org/10.1007/s10853-020-05473-x

15 Markov, P. A., Vinogradov, I. I., Kostromina, E., Eremin, P. S., Gilmutdinova, I. R., Kudryashova, I. S., Greben, A., Rachin, A. P., & Nechaev, A. N. (2022). A wound dressing based on a track-etched membrane modified by a biopolymer nanoframe: physi-cochemical and biological characteristics. *European Polymer Journal, 181*, 111709. https://doi.org/10.1016/J.EURPOLYMJ.2022.111709

16 Pereao, O., Uche, C., Bublikov, P. S., Bode-Aluko, C., Rossouw, A., Vinogradov, I. I., Nechaev, A. N., Opeolu, B., & Petrik, L. (2021). Chitosan/PEO nanofibers electrospun on metallized track-etched membranes: fabrication and characterization. *Materials Today Chemistry, 20*, 100416. https://doi.org/10.1016/J.MTCHEM.2020.100416

17 Vinogradov, I. I., Petrik, L., Serpionov, G. V., & Nechaev, A. N. (2021). Composite Membrane Based on Track-Etched Mem-brane and Chitosan Nanoscaffold. *Membranes and Membrane Technologies, 3*(6), 400–410. https://doi.org/10.1134/S2517751621060093

18 Vinogradov, I. I., Andreev, E. V., Yushin, N. S., Sokhatskii, A. S., Altynov, V. A., Gustova, M. V., Vershinina, T. N., Zin'kovskaya, I., Nechaev, A. N., & Apel', P. Yu. (2023). A Hybrid Membrane for the Simultaneous Selective Sorption of Cesium in the Ionic and Colloid Forms. *Theoretical Foundations of Chemical Engineering, 57*(4), 549–562. https://doi.org/10.1134/S0040579523040498

19 Vinogradov, I. I., Drozhzhin, N. A., Kravets, L. I., Rossouw, A., Vershinina, T. N., & Nechaev, A. N. (2024). Formation of Hybrid Membranes for Water Desalination by Membrane Distillation. *Colloid Journal, 86*(5), 667–679. https://doi.org/10.1134/S1061933X24600519

20 Rossouw, A., Olejniczak, A., Olejniczak, K., Gorberg, B., Vinogradov, I., Kristavchuk, O., Nechaev, A., Petrik, L., Perold, W., & Dmitriev, S. (2022). Ti and TiO2 magnetron sputtering in roll-to-roll fabrication of hybrid membranes. *Surfaces and Interfaces, 31*, 101975. https://doi.org/10.1016/J.SURFIN.2022.101975

21 Ivanshina, O. Yu., Zuba, I., Sumnikov, S. V., Nabiyev, A. A., & Pawlukojć, A. (2021). L-Tryptophan metal-organic frame-works based on transition metals: Preparation, characterization and application for ruthenium 3+ ions sorption. 020001. https://doi.org/10.1063/5.0063607

22 Ponomareva, O. Yu., Drozhzhin, N. A., Vinogradov, I. I., Vershinina, T. N., Altynov, V. A., Zuba, I., Nechaev, A. N., & Pawlukojć, A. (2024). Metal–Organic Framework Based on Nickel, L-Tryptophan, and 1,2-Bis(4-Pyridyl)Ethylene, Consolidat-ed on a Track-Etched Membrane. *Russian Journal of Inorganic Chemistry, 69*(6), 914–924. https://doi.org/10.1134/S0036023624600667

23 Ho, Y. S. (2006). Review of second-order models for adsorption systems. *Journal of Hazardous Materials, 136*(3), 681–689. https://doi.org/10.1016/J.JHAZMAT.2005.12.043

24 Lu, H., Yang, Q., Huang, B., Qi, J., Wang, R., Zhou, Q., Chen, Q., Zhu, L., Jin, J., & Kong, Y. (2023). Removal performance and adsorption kinetics of dyes by a Co-based metal organic framework. *Microporous and Mesoporous Materials, 360*, 112665. https://doi.org/10.1016/J.MICROMESO.2023.112665

25 Abin-Bazaine, A., Campos Trujillo, A., & Olmos-Marquez, M. (2022). Adsorption Isotherms: Enlightenment of the Phenom-enon of Adsorption. In *Wastewater Treatment. IntechOpen*. https://doi.org/10.5772/intechopen.104260

26 Sahoo, T. R., & Prelot, B. (2020). Adsorption processes for the removal of contaminants from wastewater: the perspective role of nanomaterials and nanotechnology. *Nanomaterials for the Detection and Removal of Wastewater Pollutants*, 161–222. https://doi.org/10.1016/B978-0-12-818489-9.00007-4

27 Li, X., Wang, J., Zhang, X., & Chen, C. (2015). Powdered activated carbon adsorption of two fishy odorants in water: Trans, trans-2,4-heptadienal and trans, trans-2,4-decadienal. *Journal of Environmental Sciences, 32*, 15–25. https://doi.org/10.1016/J.JES.2015.01.001